JOURNAL OF SOLID STATE CHEMISTRY 82, 247–254 (1989)

Jonker-type Analysis of Small Polaron Conductors

J. NELL AND B. J. WOOD

Northwestern University, Department of Geological Sciences, Evanston, Illinois 60208

S. E. DORRIS

Argonne National Laboratory, Materials and Components Technology Division, Argonne, Illinois 60439

AND T. O. MASON

Northwestern University, Department of Materials Science and Engineering, Evanston, Illinois 60208

Received January 19, 1989; in revised form June 14, 1989

Plots of Seebeck coefficient vs the logarithm of electrical conductivity (Jonker plots) can be used to discriminate small polaron from band-type semiconductivity. Furthermore *n*-type and *p*-type small polaron conduction can be discriminated. Examples are drawn from systems exhibiting extensive nonstoichiometry, e.g., CeO_{2-x} and $Fe_{1-x}O$, systems involving extensive doping, e.g., $LaCrO_3$: Sr and Mn_3O_4: Fe, and systems with extensive solid solubility, e.g., the spinel ferrites. Capabilities and limitations of the analysis are discussed. © 1989 Academic Press, Inc.

Introduction

Small polaron conduction can be thought of as the thermal "diffusion" or hopping of a charge carrier and its associated lattice polarization field between equivalent sites but opposing valence states, typically in variable valence compounds, e.g., compounds of transition metals, lanthanides, or actinides. In contrast to all other electronic conduction mechanisms, lattice vibrations do not reduce electron mobility, but rather enable it to take place much like for ionic conductivity. The resulting low but activated mobilities (≤ 1 cm^2 V^{-1} sec^{-1}) combined with typically large carrier concentrations ($\approx 10^{22}$ cm^{-3}) yield values of conductivity (10^0 to $10^{2.5}$ Ω^{-1} cm^{-1}) intermediate to those for normal semiconductors and metals, and often with small or negligible apparent activation energies. Materials exhibiting such conduction include technologically important oxides based upon transition metals such as Fe (e.g., spinel ferrites (*1*)), Co, Mn (e.g., PTCR thermistors (*2*)), Cr (e.g., conductive perovskites (*3*)), and lanthanides such as Ce or actinides such as U (e.g., mixed conductors (*4*)). Recently it has been suggested that new high-T_c superconducting oxides based upon the transition metal copper are also small polaron conductors in the normal state (*5*).

The distinctive features of small polaron

0022-4596/89 $3.00

conduction are apparent in the equations for conductivity and Seebeck coefficient. Given a total density of conducting sites, N, a fraction c of which are occupied by charge carriers, the Nernst–Einstein equation can be used to calculate the conductivity,

$$\sigma = (Nc)e\mu = (Nc)eD/kT, \quad (1)$$

where μ is the mobility, T is absolute temperature, e and k have their usual meanings, and D is the small polaron "diffusivity":

$$D = g(1 - c)ea^2\nu \exp[-E_H/kT]. \quad (2)$$

Here g is a geometric factor, a is the jump distance between equivalent sites, ν is a lattice vibrational frequency, E_H is the hopping energy, and $(1 - c)$ is the probability that the adjacent site is of appropriate valence for an exchange to occur. The resulting conductivity is (*6, 7*)

$$\sigma = \frac{gNc(1 - c)e^2a^2\nu}{kT} \exp\left[\frac{-E_H}{kT}\right]. \quad (3)$$

On the other hand, the small polaron Seebeck coefficient is given by (*6, 8*)

$$Q = \pm k/e \ln[2(1 - c)/c], \quad (4)$$

where all entities have been defined previously. The $\pm$ sign indicates that the small polaron can involve either a hole (p-type) or an electron (n-type). It will be demonstrated that although the sign of Q usually agrees with the type of small polaron, sign changes can occur for a given type of small polaron conduction when c is large ($\geq 2/3$).

The characteristic features of small polaron conduction are evident in Eqs. (1–4). The pre-exponential T^{-1} term (see Eq. (1)) is difficult to demonstrate unless the carrier concentration is fixed and the electrical conductivity is measured over a wide temperature range. To the authors' knowledge, the only study which was so conducted was for Sr-doped lanthanum chromite (*9*); as discussed in detail below, the Sr doping fixed the hole concentration and the wide range of experimental temperatures (RT to 2000 K) enabled the pre-exponential temperature factor to be clearly seen. The usual means for demonstrating small polaron conduction is via an activated mobility (see Eq. (2)). An activated mobility is apparent when the conductivity is activated but the thermopower is not (e.g., in CeO_{2-x} at fixed x (*6*)) and the $La_{1-y}Sr_yCrO_3$ at fixed y (*9*), when the conductivity has a significantly larger activation energy than the thermopower (e.g., in Mn_3O_4 (*9*)), and when the conductivity is analyzed at constant Seebeck coefficient in systems where both properties vary with defect content (e.g., in $Fe_{1-x}O$ (*10, 11*)). The isothermoelectric analysis technique is described in detail elsewhere (*11, 12*).

Small polaron behavior can frequently be concluded on the basis of the Seebeck coefficient alone. In systems where the carrier concentration is fixed through "freezing-in" a certain nonstoichiometry (e.g., CeO_{2-x} (*6*)) or through a predetermined doping concentration (e.g., $La_{2-y}Sr_yCrO_3$ (*9*)) small polaron conduction is evidenced by a temperature-independent Seebeck coefficient. In addition, the Seebeck coefficient can be plotted vs carrier concentration as determined from the nonstoichiometry or doping level. In both CeO_{2-x} (*6*) and $La_{1-y}Sr_yCrO_3$ (*9*) the behavior closely follows Eq. (4), the former exhibiting n-type character and the latter exhibiting p-type character. In Fe_3O_4 and its solid solutions, we have demonstrated that the variation of thermopower and conductivity with defect concentration (*7*) or with solid solution composition (*13, 14*) is consistent with changes in the octahedral site Fe^{3+}/Fe^{2+} ratio as determined by the overall cation and valence distribution. These materials obey the n-type version of Eq. (4).

In the general case, however, small polaron conduction is difficult to detect and to

confirm. Usually too small a temperature range is measured for the T^{-1} term to be clearly seen. In many instances E_H, if observed, is on the order of kT. This means that there is often an indistinguishable difference between the activation energies of conductivity and thermopower. Furthermore, there is a tendency for the T^{-1} and exponential terms in Eq. (3) to cancel. For example, Fe_3O_4 exhibits little or no temperature dependence over a broad temperature range although small polaron conduction has been confirmed on other grounds (*7*). In the general case, unless the defect structure is already known, little can be inferred from the nonstoichiometry or composition dependence of the Seebeck coefficient. There is clearly a need for an additional approach which can unambiguously establish whether or not small polaron conduction is operative in the general case.

Many years ago Jonker (*15*) developed a means of analyzing semiconducting behavior in systems which can be driven both *n*-type and *p*-type by suitable dopants. The analysis consists of a plot of Seebeck coefficient vs the logarithm of electrical conductivity which results in a "pear-shaped" figure. Such plots are usually referred to as "Jonker pears." From the size and position of a given plot considerable information can be obtained about the conduction parameters, e.g., the intrinsic band gap and the density of states-mobility product. We have extended Jonker's analysis to systems which exhibit small polaron conduction. The resulting plot of Seebeck coefficient vs the logarithm of conductivity is significantly different from that of a conventional semiconductor, especially at large carrier concentrations. In addition, completely distinct curves are obtained for *n*-type and *p*-type small polaron systems. Data of known small polaron systems (CeO_{2-x}, $Fe_{1-x}O$, $LaCrO_3$: Sr, Mn_3O_4: Fe, and the spinal ferrites) can be evaluated via Jonker-type small polaron analysis. The conditions and limitations of the technique are outlined below.

Theory

Jonker's (*15*) approach assumed a two-band model for both conductivity and Seebeck coefficient. This is necessary to describe the *n*-to-*p* transition in the intrinsic regime. Since we are concerned with the behavior at large carrier concentrations, only the extrinsic "legs" of the Jonker plot need be considered. For example, the *p*-type leg of the plot results from combining equations for conductivity,

$$\sigma_+ = pe\mu_+, \tag{5}$$

and Seebeck coefficient,

$$Q_+ = k/e[\ln(N_+/p) + A_+], \tag{6}$$

to yield

$$Q_+ = k/e \ln N_+ e\mu_+ e^{A_+} - k/e \ln \sigma_+. \tag{7}$$

Here N_+ is the density of states, p is the density of carriers, and A_+ is the transport constant. An analogous equation can be derived for the *n*-type leg:

$$Q_- = -k/e \ln N_- e\mu_- e^{A_-} + k/e \ln \sigma_-. \tag{8}$$

Under the conditions that densities of states and transport constants are the same for the two mechanisms, i.e., $N_+ = N_-$ and $A_+ = A_-$, the dashed lines in Fig. 1 with slopes $\pm k/e$ are obtained; this corresponds to the point of the Jonker "pear." The lines have each been normalized to unit conductivity at $Q = \pm 59$ μV/K in order to facilitate comparison with the small polaron curves to be derived as follows.

By defining the valence ratio, $q = c/(1 - c)$, it can be shown that this ratio can be related to the thermopower (see Eq. (4)) by the equation

$$q = c/(1 - c) = 2 \exp(+Qe/k) \tag{9}$$

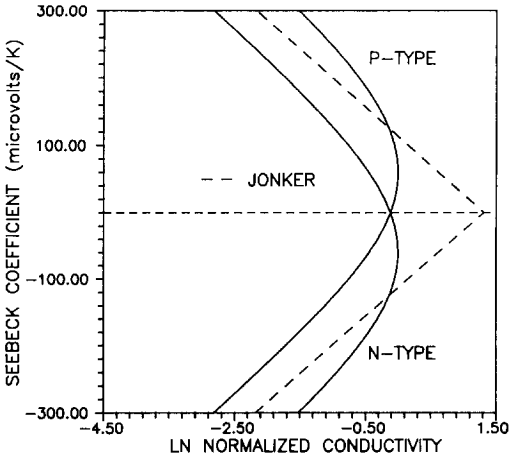

FIG. 1. Seebeck coefficient vs logarithm of conductivity for *p*-type and *n*-type small polaron systems as compared to typical semiconductor (Jonker) behavior.

for an *n*-type small polaron system or

$$q = c/(1 - c) = 2 \exp(-Qe/k) \quad (10)$$

for a *p*-type small polaron system. In either case, it can be proven that the product $c(1 - c)$ is

$$c(1 - c) = q/(1 + q)^2. \quad (11)$$

This same product can be isolated in the expression for the conductivity (see Eq. (3)),

$$c(1 - c) = (\sigma/\Omega N\nu) \exp(E_H/kT), \quad (12)$$

where it is assumed that the product $\Omega = ge^2a^2/kT$ is approximately constant at a fixed temperature. Furthermore, assuming that conduction site density (N), jump frequency (ν), and hopping energy (E_H) are independent of nonstoichiometry, doping, or solid solution composition, it follows from Eq. (3) that the maximum conductivity will occur at $c = 0.5$. We can therefore normalize the $c(1 - c)$ product to the value at the maximum conductivity as

$$c(1 - c)/(0.5)^2 = \sigma/\sigma_{max}. \quad (13)$$

By combining this equation with Eq. (11) and either Eq. (9) (*n*-type) or Eq. (10) (*p*-type) the small polaron curves of Fig. 1 are obtained. Here the conductivity is normalized to σ_{max}, the conductivity at $c = 0.5$ where $Q = \pm 59\ \mu V/K$.

It is clear from Fig. 1 that small polaron behavior will most clearly manifest itself in the vicinity of the maximum conductivity. This requires sufficient carrier concentrations to result in absolute thermopower values less than approximately 150 $\mu V/K$ ($c \geq 0.26$) such that curvature becomes noticeable in the small polaron plots. Otherwise, as at small carrier concentrations, linear behavior is obtained with slopes of $\pm k/e$ regardless of mechanism, whether band-type or small polaron. Under such conditions the mechanism cannot be determined from a given Jonker plot alone. (It *is* possible to infer small polaron conduction from the high conductivity intercept, given additional information about the carrier concentration, e.g., from Hall measurements, or from a positive temperature dependence of the intercept on a series of isotherms due to an activated mobility. See Refs. (*15*) and (*16*) for a discussion and examples.)

Results and Discussion

Data for the systems CeO_{2-x} (*6*) and $Fe_{1-x}O$ (*17*) have been plotted in Jonker fashion in Fig. 2. For comparison, both *p*-type and *n*-type small polaron curves have also been plotted. It is interesting to note that both systems undergo changes in the defect structure as the oxygen-to-cation ratio is varied. This results in changes in the concentrations of the valence states responsible for conduction. As can be seen, both systems follow the *n*-type small polaron behavior.

In CeO_{2-x} the defect structure has been interpreted as consisting of oxygen vacancies charge compensated by Ce^{3+} species which are small polaron electrons (*6*). As the deviation from stoichiometry increases, the absolute value of the Seebeck coeffi-

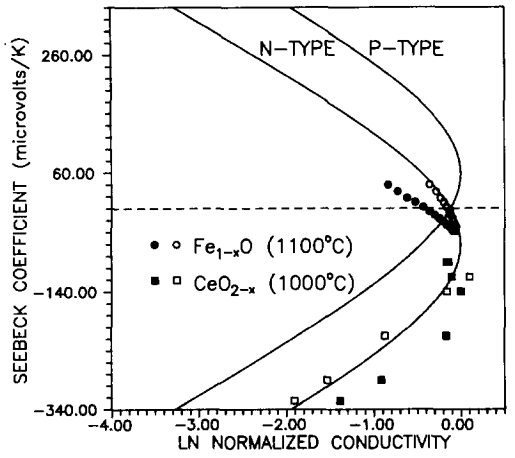

FIG. 2. *N*-type small polaron Jonker plots for CeO_2 (*6*) and FeO (*17*). The raw CeO_2 data (closed squares) have been corrected for changes in the $N\nu$ product (*10*) (open circles).

cient decreases and the conductivity increases and then becomes relatively constant. As can be seen in Fig. 2, this does not agree completely with *n*-type behavior. This discrepancy can be explained if the increase in hopping energy at large deviation from stoichiometry (*6*) is taken into account. We have corrected the original data for the changes in hopping energy (see Eq. (12)) and the results are the open squares in Fig. 2. The agreement with *n*-type small polaron behavior is now acceptable.

The electrical properties of FeO have long been enigmatic. We have shown that the change in sign of the thermopower is not associated with a change in mechanism, but rather with a monotonic change in the Fe^{3+}/Fe^{2+} ratio on conducting sites as the nonstoichiometry is varied (*11*). Furthermore, although Fe^{3+} is overall a minority species, its concentration adjacent to vacancy-interstitial clusters can approach 50%. It is on these sites that hopping conduction takes place via cluster-to-cluster percolation. (See Refs. (*18, 19*) for a description of the defect structure and conduction model, respectively.) What Fig. 2 illustrates conclusively is that FeO is an *n*-type small polaron conductor. Even before correcting for the dependence of the $N\nu$ product with nonstoichiometry, it can be seen that the first derivative of the raw data in Fig. 2 is inconsistent with *p*-type behavior but consistent with *n*-type behavior. In Ref. (*11*) we published the variation in the conduction site density-jump frequency product with composition. (The hopping energy was composition independent). When the raw data are appropriately corrected for the change in $N\nu$ with nonstoichiometry, excellent agreement with the *n*-type curve is obtained.

In Fig. 3 raw and corrected data for the systems $La_{1-y}Sr_yCrO_3$ (*9*) and $Mn_{3-y}Fe_yO_4$ (*20*) have been plotted against the *n*-type and *p*-type small polaron curves. These systems can be characterized as extensively doped materials, although the Mn_3O_4 : Fe case can also be discussed in the context of solid solution systems (see below). It is clear that these data exhibit *p*-type small polaron behavior.

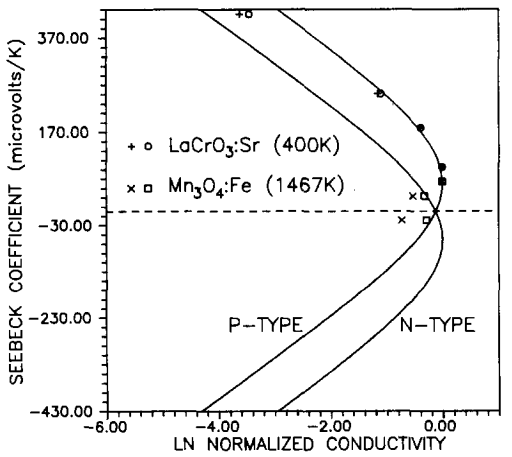

FIG. 3. *P*-type small polaron Jonker plots for La CrO_3 : Sr (*9*) and Mn_3O_4 : Fe (*20*). The raw $LaCrO_3$: Sr data (closed circles) have been corrected for changes in hopping energy (open circles). The raw Mn_3O_4 : Fe data (closed squares) have been corrected for changes in the density of conducting sites (open squares).

The defect chemistry in $LaCrO_3$: Sr has been interpreted as $La^{3+}_{1-y}Sr^{2+}_yCr^{3+}_{1-y}Cr^{3+}_yO_3$, with Sr^{2+} residing on La^{3+} sites charge compensated by Cr^{4+} on Cr^{3+} sites (*9*). The $[Cr^{4+}_{Cr^{3+}}]$ species are small polaron holes according to our analysis. Both pre-exponential and exponential (hopping energy) factors were virtually composition independent in the system according to Ref. (*9*). Furthermore, since no dilution of conducting sites is taking place, the conduction site density (N) should be invariant. This explains why the raw data are in such good agreement with the predicted behavior.

The Mn_3O_4 : Fe data (*20*) are published here for the first time. By analogy to the $Fe_{1-x}O$ raw data, which exhibited n-type behavior by virtue of a negative slope at the sign change of thermopower, it can be argued that these data exhibit p-type behavior by virtue of a positive slope at the sign change of thermopower. Although jump frequency and hopping energy do not change significantly with composition in the Mn_3O_4 : Fe system, the octahedral Mn^{4+} and Mn^{3+} species are being diluted by the Fe doping. We have corrected for this according to Eq. (12) and the results are in good agreement with the p-type curve.

The defect/valence structure of Mn_3O_4 : Fe is extremely complex. We have interpreted the high temperature electrical properties of cubic Mn_3O_4 (8) as being consistent with substantial disproportion of octahedrally coordinated Mn^{3+} into Mn^{2+} and Mn^{4+} and that small polaron conduction takes place between Mn^{4+} (small polaron holes) and Mn^{3+}. In the solid solution, Fe incorporates almost exclusively as Fe^{3+} and primarily on octahedral sites out to the composition $y = 0.8$ in $Mn_{3-y}Fe_yO_4$ (*20*). See Ref. (*20*) for a complete discussion of the Mn_3O_4–Fe_3O_4 solid solution which exhibits a change in mechanism from p-type small polaron near Mn_3O_4 to n-type small polaron near Fe_3O_4.

The systems considered to this point exhibit only small variations in the parameters N, ν, and E_H with nonstoichiometry or doping. In extensive solid solutions exhibiting small polaron conduction this need not be the case. In Fig. 4 are plotted raw and corrected data for Fe_3O_4 and the solid solutions $(1 - x)Fe_3O_4$–$xM_gFe_2O_4$ and $(1 - x)Fe_3O_4$–$xFeAl_2O_4$ (*21*). As can be seen, the raw data exhibit marked deviations from the behavior predicted for n-type small polarons. The dashed lines are merely guides for the eye, but illustrate that conductivity falls off dramatically as one proceeds from $x = 0$ (pure Fe_3O_4) to $x = 0.25$, 0.50, and 0.75. There are two factors primarily responsible for the large deviations. First, the octahedral Fe^{2+} (the small polaron electrons) and octahedral Fe^{3+} (the available conduction sites) are being severely diluted as x increases due to Mg^{2+} or Al^{3+} substitution. Second, the hopping energy increases significantly for both solid solutions as x increases. From our detailed analysis of the cation distributions and conduction parameters in these two solutions (*21*) we have corrected the data for changes in N and in

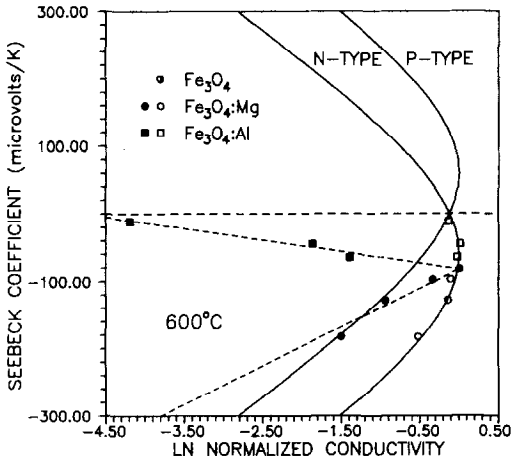

FIG. 4. N-type small polaron Jonker plot for Fe_3O_4 and spinel ferrites. Raw data (closed points) have been corrected for changes in hopping energy and the density of conducting sites (open points).

E_H with composition. As can be seen in the figure, the agreement with the *n*-type curve is now quite satisfactory.

These examples of "narrow band" small polaron behavior illustrate the utility of Jonker-type analysis for small polaron systems. It must be pointed out, however, that not all systems behave in such an ideal fashion. As initially pointed out by Emin (*22*), where structural disorder occurs such as in amorphous semiconductors or where hopping occurs between inequivalent sites, an energy band of small polaron states occurs resulting in an additional term which is approximately linear in temperature such that

$$Q = \alpha + \beta T, \qquad (14)$$

where β has the same sign as α and α is essentially the standard configurational entropy term expressed by Eq. (4). Examples of such behavior are found in the systems $B_{1-x}C_x$ (*23*), $Li_{1+x}Ti_{2-x}O_4$ (*24*), and $Y_{1-x}M_xCrO_3$ (*25*). Unless β is a well-behaved function of composition, the Jonker plot for such a system will be entirely unpredictable. In the case of $Y_{1-x}M_xCrO_3$ (M = Mg, Ca, Sr, or Ba) β differed from dopant to dopant but was in each case composition-independent. In such a case the Jonker plot will maintain its shape but be shifted by βT away from the x-axis.

The examples we have chosen illustrate the capabilities and limitations of Jonker-type analysis for small polaron systems. Curvature at large carrier concentrations, i.e., for low absolute values of thermopower, can be taken as diagnostic for small polaron conduction. The sign of thermopower at the nose of the curve indicates the sign of the polaron, whether *n*-type or *p*-type. Unfortunately, the analysis requires that conduction parameters such as conduction site density (N), jump frequency (ν), and hopping energy (E_H) be independent of the carrier concentration. Since isothermal changes in carrier concentration are accomplished by extensive changes in anion-to-cation stoichiometry, doping, or solid solution, this is rarely the case. It is possible, however, to correct the data for changes in these parameters. In exceptional cases, where site disorder or inequivalence arises, an additional term must be included in the model for thermopower. This may or may not result in unpredictable Jonker plot behavior.

Acknowledgments

This work was supported by DOE Grant FG02-84ER45097. The spinel ferrite work was supported by NSF Grant EAR-8618340. The help of M.-Y. Su with the figures is greatly appreciated.

References

1. K. J. Standley, "Oxide Magnetic Materials," Oxford Univ. Press (Clarendon), London/New York (1972).
2. H. B. Sachse, "Semiconducting Temperature Sensors and Their Application," Wiley, New York (1975).
3. J. Mizusaki, T. Sasamoto, W. R. Cannon, and H. K. Bowen, *J. Amer. Ceram. Soc.* **65**(8), 363 (1982).
4. H. L. Tuller, *in* "Nonstoichiometric Oxides" (O. T. Sorensen, Ed.), Academic Press, New York (1981).
5. M.-Y. Su, K. Sujata, and T. O. Mason, *in* "Ceramic Superconductors II" (M. F. Yan, Ed.), pp. 99–114, Amer. Ceram. Soc., Columbus, OH (1988).
6. H. L. Tuller and A. S. Nowick, *J. Phys. Chem. Solids* **38**, 859 (1977).
7. R. Dieckmann, C. A. Witt, and T. O. Mason, *Ber. Bunsen-Ges. Phys. Chem.* **87**(6), 495 (1983).
8. S. E. Dorris and T. O. Mason, *J. Amer. Ceram. Soc.* **71**, 379 (1988).
9. D. P. Karim and A. T. Aldred, *Phys. Rev. B* **20**(6), 2255 (1979).
10. E. Gartstein and T. O. Mason, *J. Amer. Ceram. Soc.* **65**(2), C-24 (1982).
11. H.-C. Chen, E. Gartstein, and T. O. Mason, *J. Phys. Chem. Solids* **43**(10), 991 (1982).
12. T. O. Mason, *Physica B* **150**, 37 (1988).
13. C. C. Wu, S. Kumarakrishnan, and T. O. Mason, *J. Solid State Chem.* **37**, 144 (1981).
14. T. O. Mason, *J. Phys. Chem. Miner.* **14**, 156 (1987).

15. G. H. JONKER, *Phillips Res. Rep.* **23,** 131 (1968).
16. M.-Y. SU, C. E. ELSBERND, AND T. O. MASON, *J. Am. Ceram. Soc.*, in press.
17. W. J. HILLEGAS, Ph.D. Thesis, Northwestern University, Evanston, IL (1968).
18. E. GARTSTEIN, T. O. MASON, AND J. B. COHEN, *J. Phys. Chem. Solids* **47**(8), 759 (1986).
19. E. GARTSTEIN, J. B. COHEN, AND T. O. MASON, *J. Phys. Chem. Solids* **47**(8), 775 (1986).
20. S. E. DORRIS, Ph.D. Thesis, Northwestern University, Evanston, IL (1986).
21. J. NELL, T. O. MASON, AND B. J. WOOD, *J. Phys. Chem. Min.* **474**(3/4), 339 (1989).
22. D. EMIN, *Phys. Rev. Lett.* **35**(13), 882 (1975).
23. C. WOOD AND D. EMIN, *Phys. Rev. B* **29**(8), 4582 (1984).
24. I. MAEKAWA, F. TAKAGI, Y. SAKAI, AND N. TSUDA, *J. Phys. Soc. Japan* **56**(6), 2119 (1987).
25. W. J. WEBER, C. W. GRIFFIN, AND J. L. BATES, *J. Mater. Res.* **1**(5), 675 (1986).